Developing a 55+ BTE Commercial Heavy-Duty Opposed-Piston Engine without a Waste Heat Recovery System

Dr. Neerav Abani,

Michael Chiang,

Isaac Thomas,

Nishit Nagar,

Rodrigo Zermeno

Achates Power, Inc., 4060 Sorrento Valley Blvd., San Diego, California, 92121, USA

Abstract

Heavy-duty vehicles, currently the second largest source of fuel consumption and carbon emissions are projected to be fastest growing mode in transportation sector in future. There is a clear need to increase fuel efficiency and lower emissions for these engines. The Achates Power Opposed-Piston Engine has the potential to address this growing need. In this paper, results are presented for a 9.8L three-cylinder OP Engine that shows the potential of achieving 55% brake thermal efficiency (BTE), while simultaneously satisfying emission targets for tail pipe emissions. The Achates Power OP Engines are inherently 20% more cost effective. The OP Engine architecture can meet this performance without the use of waste heat recovery systems or turbo-compounding and hence is the most cost effective technology to deliver this level of fuel efficiency.

The Achates Power OP Engine employs currently available engine components, such as supercharger, turbocharger and after-treatment and features a uniquely designed piston bowl shape to enhance mixing with a swirl-to-tumble conversion as the piston bowls approach minimum volume. This design improves fuel-air mixing and hence, results in low soot values, higher indicated thermal efficiency (ITE) due to better combustion phasing because of faster mixing controlled combustion and lower NO_x due to lower fueling requirement because of two-stroke and more efficient combustion system. The OP Engine has a lower heat transfer loss due to the inherent design of the combustion chamber, which provides lower surface area-to-volume ratio compared to a conventional engine. This results in further benefits of reduction in fuel consumption and green house gases (GHGs).

The Achates Power OP Engine also makes use of internal exhaust gas recirculation (EGR) by using an optimized design of intake and exhaust ports that improves scavenging. This reduces engine-out NO_x along with lower requirement of flowing external EGR and hence reduction in pumping requirement. 1-D and 3-D-CFD models developed for the analysis were correlated to the Achates Power 4.9L OP Engine dynamometer measured data. The correlated models were used as tools to make predictions for the 9.8L heavy-duty engine. The optimized system include high trapped compression ratio piston bowl, ports design to provide best scavenging performance, thermal barrier coating on piston bowls and dual injector with having an optimized spray pattern layout. Results show that the OP Engine results in a BTE of 55%, while meeting stringent emission standards without the use of expensive waste heat recovery systems and/or turbo-compounding components. The Achates Power OP Engine offers a solution to the automotive industry in providing a commercially viable, highly efficient and clean heavy-duty diesel engine that will reduce GHGs and carbon footprint for heavy-duty vehicles such as Class 8 trucks.

Introduction

Heavy-duty trucks are the second largest and fastest growing segment of the U.S. transportation industry. Globally, emissions from heavy-duty vehicles are growing at a faster rate that is expected to surpass emission from passenger vehicles by 2030 [1]. As the fuel consumption from Class 8 Trucks using heavy-duty engines are expected to increase in the future; the need for commercially viable, clean and highly efficient heavy-duty engines is key to reducing GHGs.

The United States Department of Energy has a currently in-progress Super-Truck Program [2] with industry partners with an objective to demonstrate 55% brake thermal efficiency by year 2020 [3,4,5,6]. Within the scope of the program, industry partners Cummins, Volvo, Navistar and Detroit Diesel have predicted BTE by simulating technologies for the future that include a waste heat recovery (WHR) system, advances in material that includes thermal-barrier coatings (TBC) to reduce heat transfer losses, friction improvement, combustion improvement that includes optimized piston bowl shape and injectors, and alternate fuel cycles. While several of these technologies have additional cost associated with it, they have demonstrated in simulations respective contribution in reducing fuel consumption. In the area of alterative combustion strategies, Hanson et al. [7] and Kokjohn et al. [8] investigated fuel reactivity in a heavy-duty engine and were able to maximize indicated thermal efficiency in a single cylinder research engine. Similar concept was extended to investigate performance of reactivity controlled compression ignition on heavy-duty multi-cylinder engine [9] and obtained around 47% BTE. Menente et al. [10] investigated various fuels in a modified Scania 13L-1 heavy-duty single cylinder research engine and obtained at certain boost pressure and EGR levels indicated efficiency between 52-55%.

Efforts from the Department of Energy, EPA and the industry are directed towards practical solutions to develop a highly efficient and clean heavy-duty engine for Class 8 trucks. The goal to achieve 55% brake thermal efficiency, while simultaneously meeting emissions standards for year 2020 will likely involve additional technologies, which will add to the cost and additional components of the vehicle. Minimizing components and cost of the engine under this objective will be crucial for a developing a commercially viable engine for heavy-duty vehicles.

Opposed-Piston Engines, currently in development at Achates Power, are lighter and more cost effective compared to conventional four-stroke engines and have potential for reductions in fuel consumption for various applications [12-16]. Achates Power OP Engines offer a solution in meeting objectives for achieving high BTE as well as meeting emissions standards without the use of waste heat recovery system and turbo-compounding. The fundamental benefits of OP Engines are discussed in detail by previous researchers [17]. A key summary of benefits of the OP Engine architecture in achieving high BTE and clean emissions compared to a conventional four-stroke engine are as follows:

1. OP Engines have lower heat transfer losses as there is no cylinder head and the combustion chamber volume at the minimum volume is encompassed by the two opposed piston bowl.
2. Due to lower a BMEP requirement to achieve similar brake-power requirement as that of conventional four-stroke engine, OP Engines operate leaner at a similar engine boost level. This results in higher thermo-dynamic efficiency due to the higher ratio of specific heat. OP Engines have larger combustion chamber volume with lower area-to-volume ratio for a given fuel amount.

3. Achates Power OP Engines include a piston bowl shape [18] that result in a enhanced mixing of fuel-spray and in-cylinder air motion, using both swirl and tumble components of flow. This leads to a faster heat released rate due to shorter mixing, controlled combustion duration and optimized combustion phasing, which maximizes indicated thermal efficiency.
4. The opposed-piston engine flow, as an open-flow device during the scavenging process, introduces a fresh charge motion and does not have a dedicated pumping stroke like conventional four-stroke engines. This helps to optimize air handling components sizing resulting in lower pumping losses. Because of the overall less restrictive flow, EGR pumping is also efficient.
5. The opposed-piston engine employs dual-fuel injectors with a narrower spray angle. This helps to reduce flame-wall interactions. Due to dual injectors, better rate shaping can be achieved compared to conventional engines.
6. Along with lower BMEP requirement, OP Engines have full and independent control of internal and external cooled EGR. Intake and exhaust pressure are controlled independently of engine speed and load. This along with enhanced mixing controlled combustion leads to lower soot as well as lower engine-out NOx.
7. OP Engines have flat BTE map for wider range of loads and speeds. This enables the OP Engine to provide better transient fuel efficiency.

While above features are advantages of OP Engines over four-stroke engines, the OP Engine also has a clear advantage to a conventional two-stroke engines as follows:

1. Lower surface area-to-volume ratio.
2. Uniflow scavenging without any use of poppet valves.
3. Higher scavenging time area for reduced pumping.
4. Higher stroke-to-bore ratio for improved scavenging.
5. Use of dual injectors instead of a central injector.

In this paper, we demonstrate the pathway to deliver 55% brake thermal efficiency using an opposed-piston two-stroke heavy-duty engine. First, we present model correlation to measured dynamometer data for the Achates Power OP 4.9L multi-cylinder research engine. We discuss the design of the research engine, its air handling system and performance and emission development. Next, we extend the correlated models to predict performance for a 9.8L multi-cylinder heavy-duty OP Engine. The unique way of operating the OP multi-cylinder engine with thermal barrier coating shows a clear pathway for meeting 55% brake thermal efficiency. We also demonstrate that this engine gives close to 48% BTE at rated power conditions. Advanced technological concepts such as various waste heat recovery system have not been included in the predictions, which will always increase the BTE further. OP Engines offer a commercially viable technology for heavy-duty engines that provides 55% BTE while simultaneously satisfying current emission standards.

Achates Power OP Research Engine Specifications

The Achates Power OP single cylinder research engine has been in testing since 2012 and the three-cylinder 4.9L research engine since 2014. The multi-cylinder research engine was originally designed to accommodate air-handling components that could provide flexibility in running various operating conditions, including very high power and high torque conditions. Because of this research engine, various torque and power requirements for different applications have been met at Achates Power. More details on this OP research engine can be found in literature [1-5].

Displacement	4.9 L
Arrangement, number of cylinders.	Inline 3
Bore	98.4 mm
Total Stroke	215.9 mm
Stroke-to-Bore Ratio	2.2
Compression Ratio	15.4:1
Nominal Power (kW @ rpm)	205 @ 2200
Max. Torque (Nm @ rpm)	1100 Nm @ 1200-1600

Table 1:Multi-cylinder Achates Power OP research engine specification

Air System for the 4.9L research OP Engine

Figure 1 provides an overview of the air-path for the three-cylinder AP OP diesel engine. Upstream of the engine, a compressor driven by a fixed-geometry turbine is used to draw in fresh air. To aid the airflow across the engine, there is a supercharger driven by a two-speed drive that allows it to run at two different crank-speed ratios. A supercharger bypass valve is used to control the airflow across the engine. The supercharger also acts as a pump to pull in the exhaust gases along the EGR loop. A venturi in the EGR loop, with a delta-pressure sensor mounted across it is used to measure the EGR mass-flow. An EGR valve is used to control the EGR flow to the engine. Downstream of the engine, a back-pressure valve is used to simulate the back-pressure of a clean after-treatment system

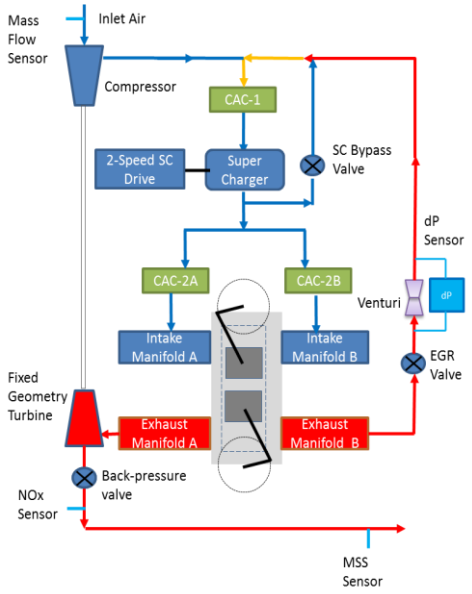

Figure 1: OP 4.9L research engine air handling system

Simulation Methodology

OP simulations essentially include scavenging process, combustion and coupling the multi-dimensional models with a one-dimensional model of OP Engine. Accurate predictions of performance and emissions from an OP Engine depend upon the accuracy of prediction of trapped conditions. Trapped conditions can be decomposed into trapped flow conditions and trapped thermo-dynamic conditions. Trapped flow conditions comprise of three-dimensional velocity distribution inside the cylinder at the instant of port closure timing, as well as kinetic energy and turbulent dissipation distribution representing trapped turbulence. Trapped flow conditions are obtained by 3-D CFD modeling of the scavenging process. Turbulence is modeled through RNG k-e model which has been widely used in engine combustion simulation. The scavenging results from 3-D CFD are passed onto 1-D developed using commercial solver GT-POWER. These 1-D models predict trapped thermodynamic conditions, viz, trapped pressure, trapped temperature and trapped composition. Trapped thermo-dynamic and trapped flow parameters are passed onto 3-D CFD engine combustion model.

To predict performance of the engine at a particular load and speed, essentially a three iteration loop calculation is carried out as shown in Figure 2 to accurately predict performance and emission parameters, such as NO_x and soot emission, indicated thermal efficiency (ITE), cylinder pressure trace and burn duration. In the first iteration, boundary conditions are created from 1-D tool in order to have boundary conditions to simulate scavenging process using 3-D-CFD. In the second iteration, the results of scavenging CFD feeds back to 1-D tool to update the 1-D prediction for trapped conditions. Next, trapped thermo-dynamic conditions are passed onto combustion CFD model. Trapped flow conditions are obtained from scavenging study in iteration-1. Typically, at second iteration, a swirl sensitivity study or a design of experiments (DOE) study is performed that finalizes the port orientation angle that determines the trapped swirl. New port geometries are constructed again in order to achieve desired target swirl. Iteration-3 is needed to predict updated scavenging parameters based on the new port orientation using 3-D-CFD scavenging simulation. Once the trapped flow field and thermo-dynamic trapped parameters are updated, the engine combustion is simulated using 3-D-CFD scavenging simulation as well as 1-D tool predictions based on the new geometry and updated trapped conditions.

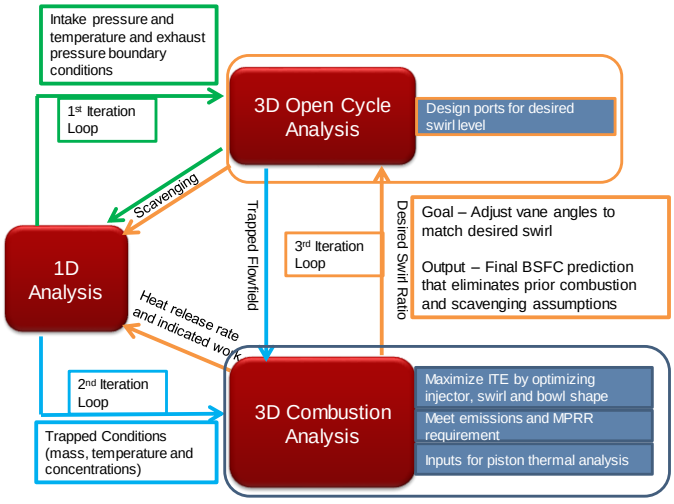

Figure 2: Schematic illustrating process of performance and emission optimization

In the case of 3-D-CFD correlation, one-way interaction between 3-D-CFD scavenging simulation and 1-D simulation is considered in order to predict trapped flow and thermo-dynamic conditions. Based on these calculated trapped parameters, a combustion CFD correlation exercise is carried out. The combustion CFD model includes a sub-model for sprays which has model constants specifically anchored to simulate spray characteristics for the injector. These constants vary and are calibrated for each injector manufacturer. These model constants depend upon various nozzle hole parameters, such as L/D ratio, k-factor and discharge coefficient. For combustion correlation, performance parameters such as engine-out NO_x and soot emissions, ITE, cylinder pressure trace and burn duration are considered as essential metrics.

CFD Model Description

A modified version of the commercially available CONVERGE CFD software version 2.2 [19] is used to perform in-cylinder simulations of the OP combustion system. The modifications to the standard version of CONVERGE2.2 include user defined functions for simulating opposed-piston two-stroke motions, and computation of several performance, emissions and thermal management sub-models. *Figure 3* shows the CAD of the API 4.9 L three-cylinder engine used in scavenging simulations. Figure 4 shows the surface geometry of the closed-cycle or combustion-cycle model with intake and exhaust pistons at their maximum separation for the third cylinder. This is because open-cycle simulations starts and ends from port-closure timing for the third cylinder for the entire 360 degree cycle. This is repeated until the open-cycle simulation converges, which is when a converged trapped flow field is obtained. This trapped flow field is used as initial flow field for the closed-cycle simulation. The trapped pressure is specified based on the cylinder pressure measurements, and the trapped composition and temperature are obtained from correlated 1-D model for 4.9L multi-cylinder engine model to measurements using one-dimensional GT-POWER model predictions, as discussed before. Note that CONVERGE generates a volume mesh automatically at every time step. Both adaptive mesh refinement and fixed grid embedding techniques [17, 19] are employed to sufficiently resolve gradients in the flow-field and essential flow features.

To simulate engine combustion, an ERC n-heptane reduced chemistry mechanism was used to solve combustion chemistry which simulates n-heptane as a diesel fuel surrogate with 35 species and 77 reaction steps [20]. NO_x is calculated from a reduced NO_x mechanism [21] based on the GRI detailed NO_x reaction mechanism [22] sub-mechanism. Soot emissions are modeled using a two-step model, which includes a Hiroyasu formation step with acetylene as the precursor [23], and a soot-oxidation step based on Nagel-Strickland equation [24]. Sprays are modeled using a modified KH-RT breakup model with RT break-up imposed in the near nozzle region as well along with a separate collision mesh for calculations for collision and coalescences [25,26]. The outcome of collisions are modeled using O'Rourke collision model [26, 27] and in-cylinder turbulence is modeled using the RNG k-ε model [28]. Fuel injection rate profiles are specified based on measured data from a state-of-the-art, in-house fuel laboratory with IFR (Injection Flow and Rate) capabilities [29]. Similar to previous work on grid sensitivity studies for standard spray models [30], in this study as well mesh resolution in the range of 2 mm throughout the domain provided adequate qualitative and quantitative agreement with measured data, as well as the best optimum runtimes to achieve accurate correlation.

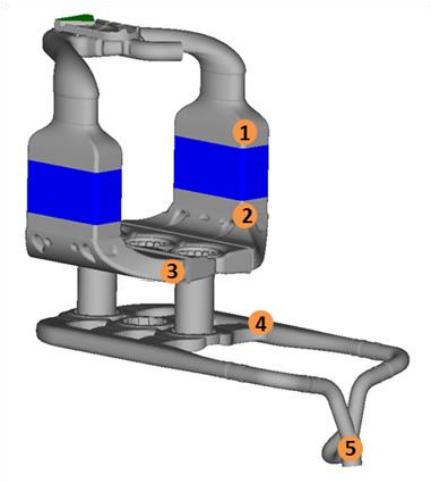

Figure 3 API 4.9L multi-cylinder engine geometry considered for scavenging simulation. Label numbers are location of high speed pressure sensors.

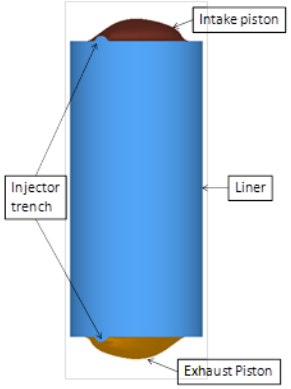

Figure 4 Closed cycle geometry to simulate combustion CFD for 3rd cylinder.

Air System Development

The air system development for the OP Engine includes designing air handling components and liner geometry. The air system of the multi-cylinder engine is developed by a coupling of 1-D models using GT-POWER and 3-D scavenging CFD model using CONVERGE2.2. Essential components of the OP Engine that are designed through analysis as part of air system development are follows:

1. Super charger: This is used for controlling mass flow to be delivered to each cylinder and hence, trapped air-fuel ratio.
2. Super charger drive: This is designed for optimizing the pumping requirement for a given load-speed condition. For operating at peak efficiency at multiple load-speed conditions, the super charger may include a 2-speed drive.
3. Compressor: This is needed to find most appropriate compressor size in order to operate at maximum efficiency range.
4. Fixed geometry turbine: This is designed for most efficient pumping and the ability to deliver back pressure and mass flow rate.
5. Liner and port geometry: Both intake and exhaust port heights are designed based on the requirement of scavenging time area and blow-down time area for a given compression-ratio and expansion ratio. Port inclination is also designed in order to achieve required trapped swirl motion that comes out from simulation of open-cycle.

Scavenging simulations for the multi-cylinder is carried out by imposing inflow boundary conditions at a location inside an intake manifold pipe just before the air cooler and outflow boundary conditions at the exhaust-turbo inlet. In case of model correlation to experiments, these locations have high speed pressure sensors that provide transient pressure measurement. In case of model predictions, these boundary conditions are provided by the 1-D model which is solved in GT-POWER.

Performance and Emissions Development

Performance and emission development is based on CFD simulations of a closed-cycle and includes designing the following combustion hardware:

1. Combustion chamber shape
2. Combustion volume to design required trapped compression ratio
3. Injector spray inclusion angle for dual injectors
4. Injector hole size
5. Number of injector holes
6. Port orientation angle to achieve required trapped swirl ratio needed for efficient and clean combustion.

As discussed previously, engine combustion is simulated using reduced chemistry mechanism and is simulated from port-closure to port-opening timings for closed-cycle simulations. This is performed for the third cylinder of the multi-cylinder engine. Trapped thermo-dynamic and trapped flow parameters are passed onto the 3-D CFD engine combustion model after convergence of 3-D CFD and 1-D simulation results. A design of the experiment is undertaken to optimize combustion system for maximum ITE that can also satisfy emission requirements.

Results and Discussion

Results are presented in two sub-sections next. First, results are presented for CFD model correlation to measurement data for the OP 4.9L engine. The measurements were conducted at Achates Power's multi-cylinder engine test dynamometer. In the second sub-section, we present the combustion performance and brake thermal efficiency predictions for the 9.8L engine using the correlated model.

Results: CFD model correlation to 4.9L research OP Engine dynamometer measurements

Achates Power's CFD model has been well correlated to the three-cylinder 4.9L OP research engine. In this sub-section we present results of open-cycle CFD correlation and combustion CFD correlation to the measurement data for the 4.9L engine. Although we present CFD correlation, the process described in the previous section where CFD and 1-D models are coupled, has been used to design hardware that has been used in the 4.9L research engine dynamometer testing. The developmental process of CFD led hardware design, CFD correlation and CFD model improvements has evolved with several cycles for wide range of hardware testing as well as wide range of OP Engine sizes. These models have continued to provide accurate performance predictions of OP Engines for various applications. Achates Power Opposed-Piston specific models have demonstrated that combustion hardware designed based on these models has resulted in measurements that were in agreement with predictions in the design stage. In this section, we present the correlation of these Achates Power developed CFD models with measurement.

Open-Cycle CFD Correlation

Open-cycle CFD correlation is an important task that feeds both 1-D tool to predict accurate cycle BSFC, as well as 3-D combustion CFD models as it provides trapped flow conditions. To achieve a computationally faster solution, a CFD model without combustion chemistry mechanism is adopted. The open-cycle model includes the closed-cycle simulation as an input with an in-house model that captures transient adiabatic index during closed-cycle specific to the OP Engine architecture. This accurately predicts the in-cylinder conditions during blow-down when the exhaust port is open, as well as during scavenging when both intake and exhaust ports are open. Appendix -I describes various scavenging parameters that are used in correlation as well as comparison. Delivery ratio and trapped cylinder pressure are the measured parameters that come from measurement and can be directly compared. Figure 5-Figure 9, shows the comparison CFD predictions of pressure at various locations at intake and exhaust manifold with measured data. As can be observed the pressure data agrees well with measurement both quantitatively, as well as the trends that confirm that the

models are well correlated and can capture pressure-wave dynamics reasonably well. The predicted mass delivered to the engine was within 2% compared to measurement.

The converged CFD solution from the open-cycle also predicts the trapped swirl motion, which is the trapped flow field required for 3-D CFD combustion simulations. Results from the CFD open-cycle correlation can be summarized as a scavenging schedule as well, and passed onto a 1-D model, which provides trapped thermodynamic conditions. After convergence and correlation of the open-cycle and 1-D model to measured data, the combustion CFD correlation comes as a next step, which will be discussed in the next section.

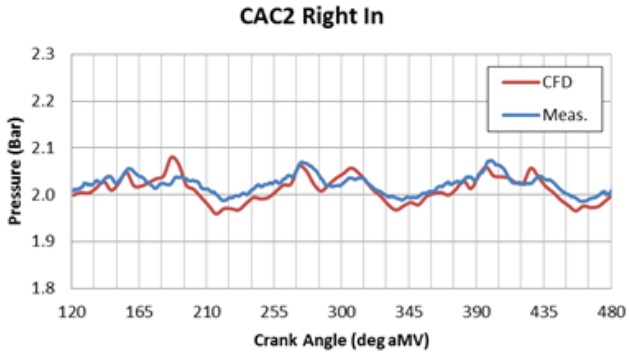

Figure 5: CFD predictions of pressure at inlet of right-side Charge Air Cooler [Location 1]

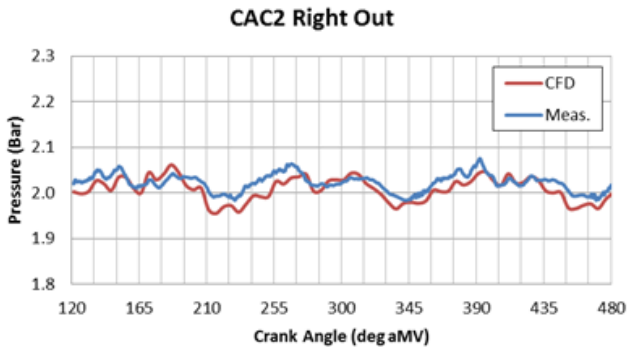

Figure 6: CFD predictions of pressure at outlet of right-side Charge Air Cooler [Location 2]

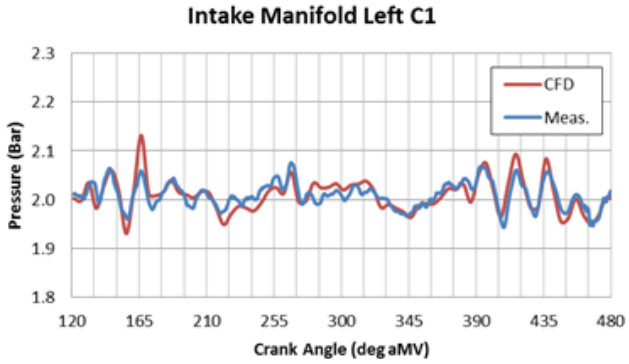

Figure 7: CFD predictions of pressure at left-side in Intake Manifold [Location 3]

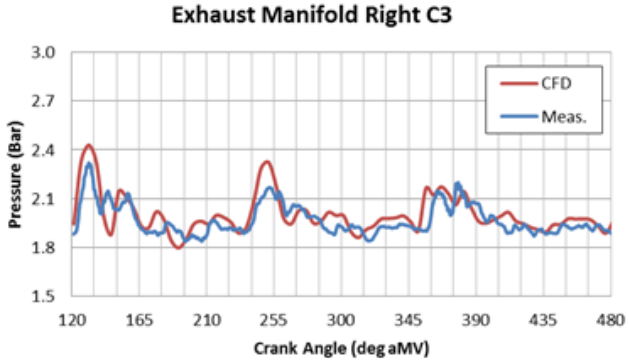

Figure 8: CFD predictions of pressure at right-side in Exhaust Manifold [Location 4]

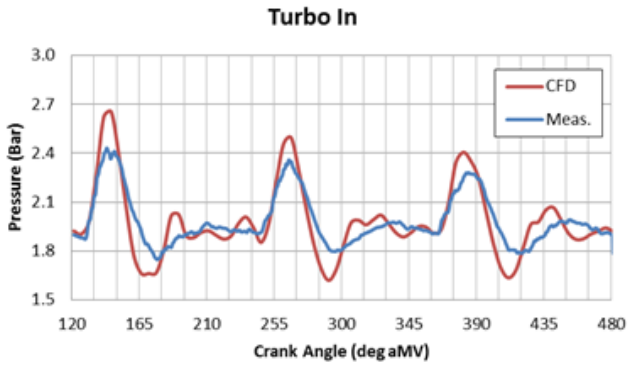

Figure 9: CFD predictions of pressure at inlet of Turbine [Location 5]

Combustion CFD Correlation

Combustion CFD models are correlated at two load and speed points; 75% load at 1400 rpm (A75 mode) and 75% load at 2200 rpm (C75 mode). The spray sub-model constants essentially are specific to each injector and each OEM. The spray sub-models have been correlated based on achieving accurate emission and cylinder pressure predictions on mesh size around 2-3 mm in the domain. The soot model constants were also anchored to provide the accurate predictions of soot measurement at both these load points.

Figure 10 shows the comparison of CFD predictions of the in-cylinder pressure and instantaneous heat released rate compared to measurements at A75 mode. The measured heat released rate is apparent heat released rate and the CFD predicted heat released rate is scaled to match the apparent heat released as derived from measurements. Table 2 comparison of emissions, closed cycle work (PdV_CC), burn duration (CA10-90) and indicated thermal efficiency (ITE). NO_x, soot and ITE compare well with measurements. Similar comparison for C75 mode are shown in Figure 11 and Table 3 that also shows emission and ITE compare well with measurements.

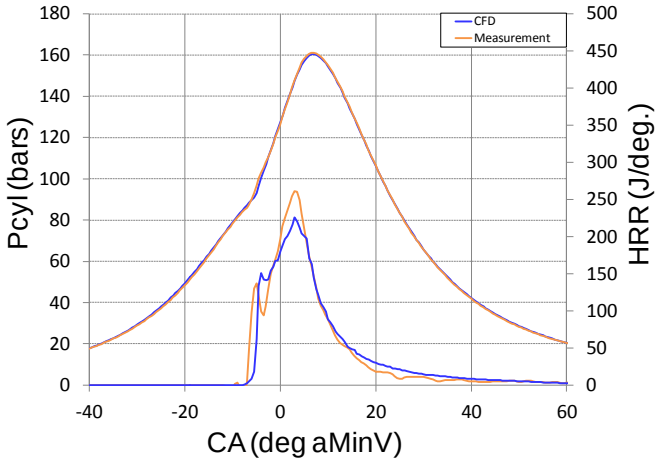

Figure 10: Comparison of in-cylinder pressure and heat released rate with measurement at A75 for API three-cylinderOP 4.9L research engine

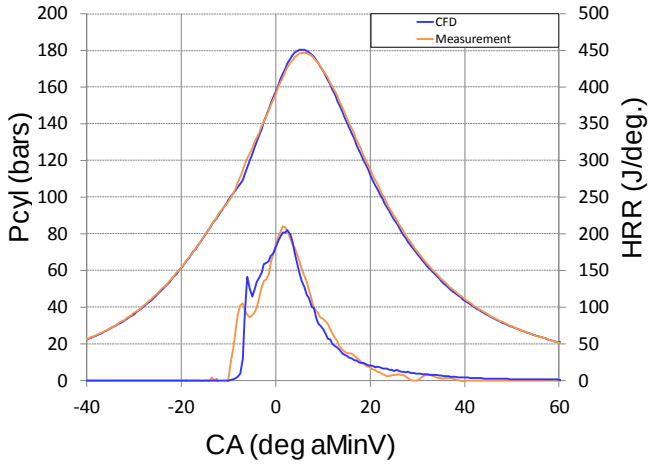

Figure 11: Comparison of in-cylinder pressure and heat released rate with measurement at C75 for the API three-cylinder OP 4.9L research engine

A75	Soot (gms/kgf)	NOx (gms/kgf)	Pdv_CC (kW)	CA10 (° ca)	CA50 (° ca)	CA90 (° ca)	CA1090 (° ca)	ITE [%]
CFD	0.077	19.9	45.2	-3.0	4.0	24.0	27.0	50.0
Measurement	0.089	19.7	45.1	-3.0	4.0	18.5	21.5	49.7

Table 2: Performance comparison of predicted vs measurements at A75 for the API three-cylinder OP 4.9L research engine

C75	Soot (gms/kgf)	NOx (gms/kgf)	Pdv_CC (kW)	CA10 (° ca)	CA50 (° ca)	CA90 (° ca)	CA1090 (° ca)	ITE [%]
CFD	0.084	10.59	62.0	-5.0	2.5	18.0	23.0	51.6
Measurement	0.082	10.53	63.2	-5.0	3.0	14.0	19.0	52.6

Table 3: Performance comparison of predicted vs measurements at C75 for the API three-cylinder OP 4.9L research engine

Friction Model Correlation

A friction model was constructed, which includes losses from the power cylinder, gearbox, crank bearings, engine auxiliaries and seals. The power cylinder and crank bearing friction was calculated using a crank angle resolved model as the shape of the in-cylinder pressure trace has a significant impact on the friction for these components.

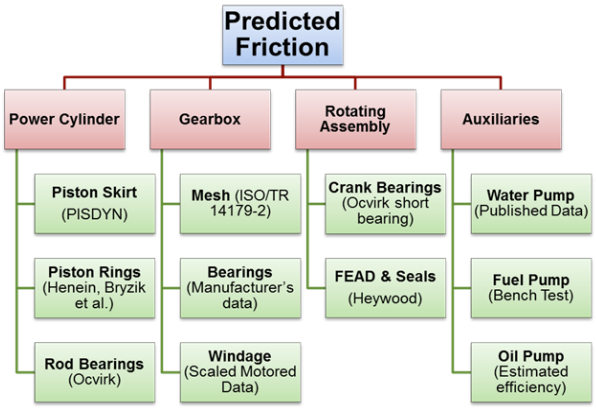

Figure 12: Overview of Friction Model

Figure 12 provides an overview of the sub-system models that were utilized in order to determine engine friction. Ricardo PISDYN was used to model piston secondary motion, dynamic land clearance and skirt friction. PISDYN includes a 3-D elasto-hydrodynamic model of the oil film between the skirt and liner and takes into account the operating conditions such as cylinder pressure, skirt geometry and skirt profile. The piston ring friction model was developed based on work published by Henien, et al [31, 32, 33]. This model accounts for transient by considering crank resolved effects for engine geometry, ring profile, liner temperature and cylinder pressure. The crank bearing model is based on short bearing theory [33, 34]. In this model the bearing loads due to gas pressure force and component inertial forces are calculated at each crank angle in order to calculate friction loss. The gear mesh losses were modeled using ISO/TR 14179-2 technical report [35]. The model calculates an average friction coefficient as a function of loading, tooth geometry, oil viscosity, surface finish and a lubricant factor. Power loss is then calculated as a function of input power, friction coefficient, and a tooth loss factor. The roller bearing losses were calculated using the data provided by the manufacturer. Geartrain windage loss was estimated using gear spin test data and a simple model was developed to scale the power loss with gear geometry

The total friction model was then compared to measured motored and the calculated fired friction of the engine in order to check its validity. An important thing to note here is that load or speed dependent constants have not been used to correlate the model results with measurement. Figure 13 shows the comparison of measured motored friction vs analytically predicted friction. As it can be seen, the model is able to predict friction within 7% of the measured motored friction.

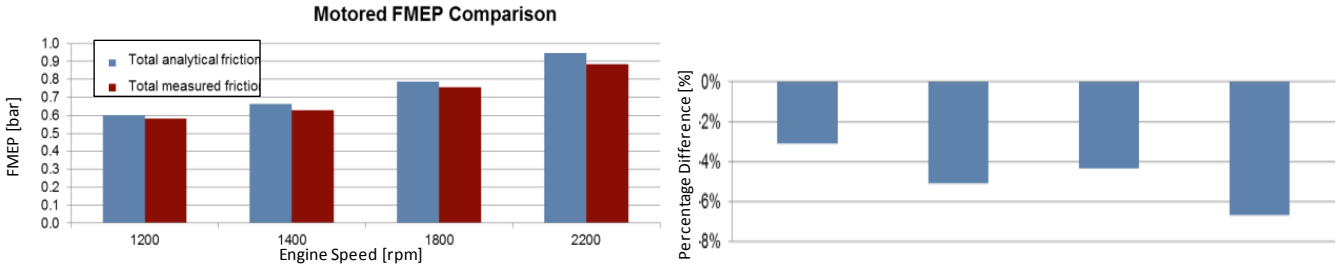

Figure 13: Comparison of measured vs predicted motored FMEP for the Achates Power 4.9L multi-cylinder research engine

The next step was to check the performance of the model in fired condition. The engine fired friction power was calculated by subtracting the supercharger power and brake power from indicated power. This was compared to the prediction from the friction model. The results are shown in

Figure 14. The analytical model is able to predict friction within +/- 10% range for most of the load speed points. The error is on higher loads, however, since friction power overall is a smaller fraction of fuel power at higher loads, the overall impact on BSFC prediction is marginal. As is evident from the measured data, the measured engine friction is high. This is because the 4.9L engine was developed as a research platform and was overdesigned with available off-the-shelf components. Some of the features that contribute to high engine friction are – an external gearbox with overdesigned gears and power take-off from central gear, oversized lube and water pump, older generation off-the-shelf ring pack, non-optimized crankshaft, bearing and a Front End Accessory Drive (FEAD).

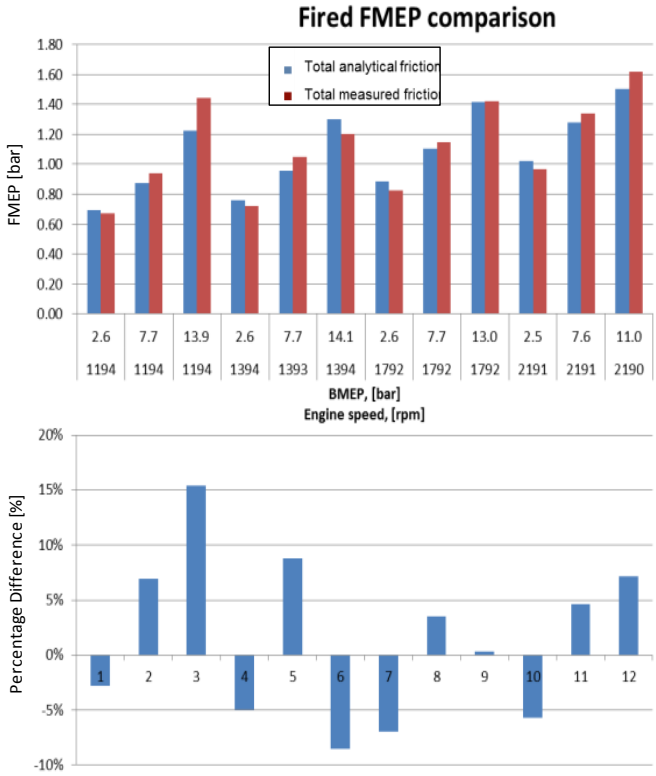

Figure 14: Comparison of analytically predicted and measured friction for Achates Power 4.9L multi-cylinder research engine

Results: API 9.8L, three-cylinder OP Heavy-duty Engine

As discussed in the previous section, the OP specific multi-dimensional models provided an excellent correlation to measured data. These models have been used for designing several engine components pertaining to air system and combustion system and have resulted in accurate predictions [15]. In this section we present predictions from these models for OP 9.8L heavy-duty engine. The predictions were made by extending the combustion CFD model used for 4.9L research engine correlation, as discussed in the previous sub-section. Due to larger mesh size requirement because of larger bore diameter, the computational time was higher since the mesh resolution was kept in the range of 2-3 mm of range during combustion event.

OP heavy-duty engine development includes developing operating conditions, designing ports that satisfy both pumping targets as well as the trapped charge motion requirements, and developing piston bowl shape and injectors to provide maximum ITE. The design process of 9.8L three-cylinder heavy-duty engine also followed the process illustrated in Figure 2. In the next sub-sections, details of scavenging optimization, port heights investigation, operating conditions for heavy-duty engine and combustion system optimization will be discussed. The engine details are shown in Table 4. Unlike a conventional four-stroke engine, the OP Engine does not need to be down-sped to deliver higher efficiency. As a result, there is not a need for a very high torque at lower RPMs, which results in simplification and cost saving for transmission and axle.

Displacement	9.8 L
Arrangement, number of cylinders.	Inline 3
Bore	120 mm
Total Stroke	288 mm
Stroke-to-Bore Ratio	2.2
Optimized Compression Ratio	21:1
Rated Power (kW @ rpm)	340 kW @ 1800
Max. Torque (Nm @ rpm)	2100 Nm @ 1200-1400

Table 4:Multi-cylinder Achates Power OP heavy-duty engine specification

The air system layout is shown in Figure 15. It is very similar to the A48-3 research engine with the addition of a low pressure EGR loop. For lower loads (50% or less), the low pressure EGR loop helps in maintaining the desired EGR rate while improving the overall turbocharger efficiency, thus lowering the pumping losses

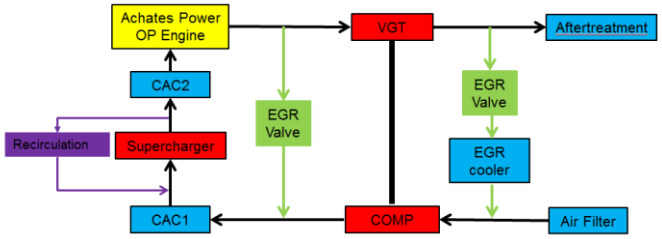

Figure 15: Air system layout for 9.8L heavy-duty OP Engine

Typically the most weighted point for a heavy-duty engine is around an engine speed of 1200 RPM and between 50-60% load. As a result, a 1200 rpm and 50% load point was chosen for the combustion system optimization and scavenging simulations to predict flow field; and, a 1-D simulation to predict the thermo-dynamic trapped conditions. DoE study to optimize combustion system was also performed at this load-speed point; details of which will be discussed in next sub-section. Further on, rated conditions were also investigated in order to ensure that the heavy-duty OP 9.8 L optimized engine also delivers 335 kW at these conditions with PCP limit of 235 bar.

Mode	Engine Speed	Power
[-]	[rpm]	[kW]
1	1200	128
2	1800	340

Table 5: OP Engine speed-load selected for combustion optimization and predictions

Scavenging Optimization

Scavenging simulations and optimization are performed with an objective of improving scavenging efficiency (SE) at maximizing trapping efficiency (TE). This is optimized along with a scavenge ratio that governs the pumping requirement of the engine. The end result of the scavenging optimization determines port height, scavenge ratio for a given load-speed point, scavenging efficiency and trapping efficiency. Typically, scavenging performance is compared for several port heights and best performing ports are investigated for its effect on combustion performance. Combustion optimization provides the requirement of trapped swirl motion that depends upon the port inclination. The outcome of combustion optimization along with scavenging optimization determines port design together.

Condition	**Port-A**	**Port-B**
RPM	1200	1200
Torque [Nm]	1022	1022
Boost [bar]	1.79	1.64
Global AFR [-]	26.0	26.1
EGR Rate [-]	29%	29%
Pumping loss [% fuel energy]	1.0	1.3

Table 6: Boundary conditions for scavenging simulations for ports

Port heights investigation

Two ports were evaluated namely port-A and port-B and have port lift profile as shown in Figure 16. Port-A are bigger ports and port-B are smaller ports. The boundary conditions for CFD simulations come from 1-D simulation results from GT-POWER tool, as shown in Table 6. The size of the ports determines the pumping, trapped temperature and the orientation determines the engine swirl. Using both the ports, combustion system was optimized and a comparison was made as to which combination of ports and combustion system provides the best ITE. Figure 17 show the boundary conditions for port-A and port-B as generated by 1-D model as part of 1st iteration. Results show that bigger ports will result in lower pumping loss but slightly lower scavenging efficiency as observed from Figure 18 and Figure 19 for the two ports, respectively. Based on data from Table 7 for scavenging performance, it can be seen that port-B results in improved scavenging, lower trapped temperature and higher trapped swirl.

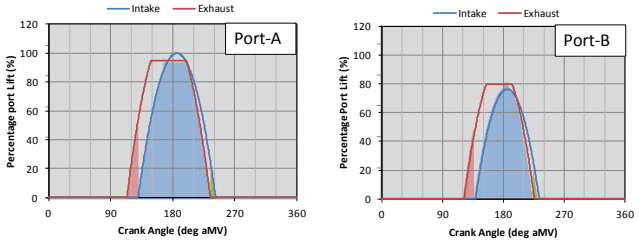

Figure 16: Port lift profile for Port-A and Port-B.

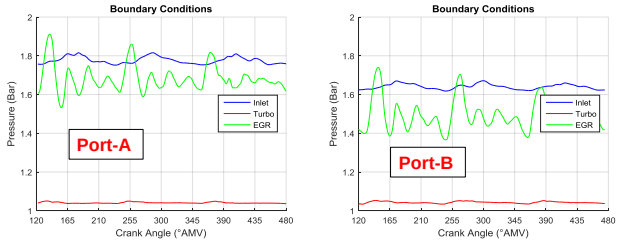

Figure 17: Transient pressure boundary conditions for scavenging simulations for two ports

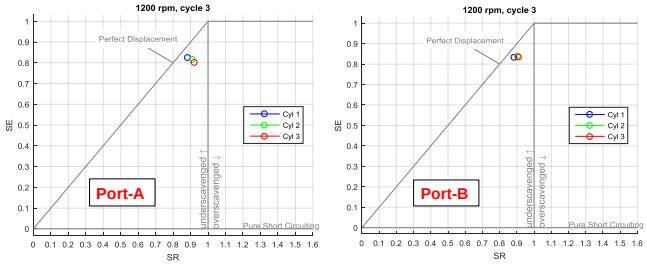

Figure 18: Scavenging efficiency for port-A and port-B.

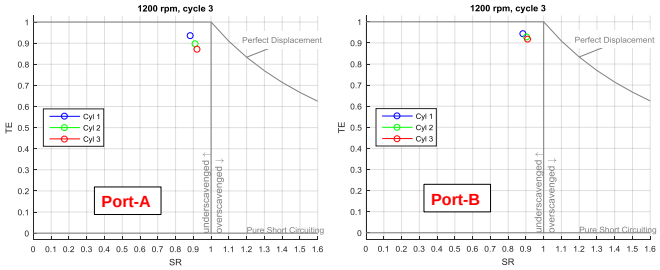

Figure 19: Trapping efficiency for port-A and port-B

Port-A 1200RPM 50%								
Description	**DR**	**CE**	**SE**	**SR**	**RC**	**TE**	**Temp@PC**	**Swirl@PC**
Unit	(-)	(-)	(-)	(-)	(-)	(-)	(K)	(-)
C1	1.051	0.984	0.825	0.882	1.192	0.936	392.6	-1.7
C2	1.084	0.972	0.816	0.910	1.191	0.897	391.7	-1.7
C3	1.060	0.923	0.802	0.921	1.151	0.871	404.1	-1.6
Average	1.065	0.960	0.815	0.904	1.178	0.901	396.1	-1.7
Range	3.0%	6.3%	2.9%	4.3%	3.4%	7.1%	3.1%	-5.1%

Port-B 1200RPM 50%								
Description	**DR**	**CE**	**SE**	**SR**	**RC**	**TE**	**Temp@PC**	**Swirl@PC**
Unit	(-)	(-)	(-)	(-)	(-)	(-)	(K)	(-)
C1	1.041	0.982	0.833	0.883	1.179	0.944	380.0	-2.4
C2	1.086	1.008	0.839	0.903	1.202	0.928	368.7	-2.4
C3	1.080	0.992	0.835	0.909	1.188	0.918	371.7	-2.4
Average	1.069	0.994	0.836	0.898	1.190	0.930	373.4	-2.4
Range	4.2%	2.6%	0.7%	2.9%	2.0%	2.8%	3.0%	-1.9%

% change	**0.4%**	**3.5%**	**2.6%**	**-0.7%**	**1.0%**	**3.2%**	**-5.7%**	**42.3%**

Table 7: Scavenging performance comparison of port-A and port-B. Definition for various terms in show in table are specified in Appendix-I.

For the combustion system a design of experiments was carried out for both the ports. It is essential to also compare combustion performance for the two ports; comparing the best combustion hardware for each port design at a range of compression ratio ranging from 15.5 to 20.5. As discussed in the previous section based on 1-D 3-D iteration after the first iteration, which provides the scavenging performance of ports; the second iteration is undertaken to improve upon boundary conditions. The improved boundary conditions are shown in Table 8 for 1200 RPM, 50% load and rated power conditions.

Speed	Torque	Power	BMEP	Global AFR	EGR	Intake Pressure
RPM	**Nm**	**kW**	**bar**	**---**	**%**	**bar**
1200	1015	128	6.5	26.4	20.4	1.8
1800	1813	340	11.6	21.8	25.0	3.2

Table 8: Boundary conditions for 1200 RPM, 50% load and rated power conditions

Combustion System Optimization

The combustion system optimization includes a design of experiment (DOE) study that optimizes piston bowl shape parameters, injector design and optimized trapped swirl ratio that will provide port inclination angle for port-B. The optimization is carried out at 1200RPM, 50% load and the resulting system is simulated at rated power conditions at 1800 rpm engine speed to predict engine performance. Commercial software MINITAB is used to construct a design of experiments model and make predictions. A range of piston bowl volume shapes were included in the study to account for range of compression ratio.

DOE study

The latest generation of the Achates Power piston bowl shape was used in the DOE study, which resulted in high indicated thermal efficiency. A 9-factor DOE with central composite (CC) design with 160 runs was used to optimize the combustion system with factors and its ranges as shown in Table 9. Figure 20 shows results from the DOE model predictor. The DOE model shows that port-B provides higher indicated thermal efficiency compared to port-A. This is primarily because of higher trapped swirl motion and lower trapped temperatures that results in higher trapped mass. Figure 21 shows validation of the DOE Model with the respective CFD predictions for indicated thermal efficiency. CFD validation of DOE predictions was necessary, especially when the DOE model selects values of factors towards the end limit of the range considered in the study. It can be seen that CFD predictions show higher indicated thermal efficiency at higher compression ratio of 19 and 20 compared to DOE model predictions. Based on these results, port-B and high compression ratio bowl combination provides maximum ITE.

DOE Factors and range for central composite design
Compression Ratio [-]
Swirl Ratio [-]
Bowl parameter 1 [mm]
Spray Inclusion Angle [deg.]
Bowl parameter_2 [mm]
Bowl parameter 3 [mm]
Hole size [mm]
Rail Pressure[bars]
Start of Injection [deg. after minimum volume (aMinV)]

Table 9: DoE Factors and range for central composite design

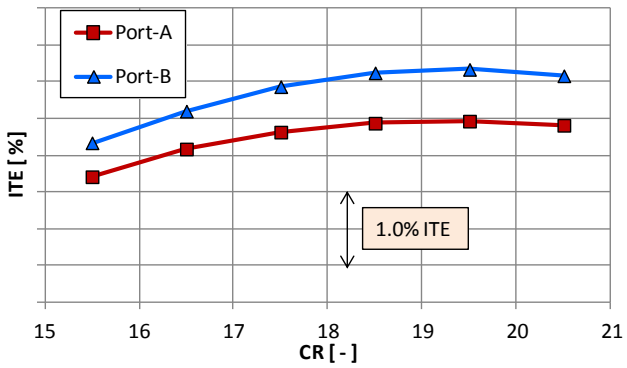

Figure 20: Combustion performance for two ports at various compression ratio

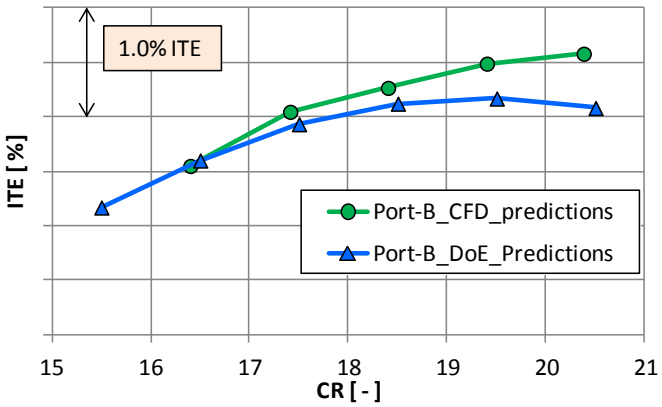

Figure 21: CFD prediction of combustion performance for port-A compared to DoE model prediction

The combustion system was optimized using a DOE model predictor for parameters at a constraint of constant engine-out NO_x. The optimized configuration for a 9.8L engine at 50% load and 1200 rpm is shown in Table 10. The DOE model predictor shows that the best configuration includes a combination of a larger nozzle hole size and a medium rail pressure based on the range considered in the study for these two factors. The optimum swirl for this condition is 2.4 and port-B geometry was re-designed with port inclination angle to provide trapped swirl ratio of 2.4 at these operating conditions. CFD predictions of ITE at various compression ratios as shown in Figure 21 show that the ITE continue to increase till compression ratio of 20.5.

Results for Optimized Operating Conditions with Combustion System Optimized for Maximum ITE

In order to maximize BTE, combination of hardware is considered which includes optimized piston bowl shape with trapped compression ratio toward higher limit, thermal barrier coating on the piston bowls and optimized injectors. SOI sweeps for this combustion system was simulated using combustion CFD at 50%load, 1200 rpm and at rated power conditions as shown in Figure 22.

Figure 23 shows the variation of ITE for the start of injection timings for the two load-speed conditions. It can be observed that advancing start of injection before 8° aMinV does not improve ITE at 50%load, 1200 rpm. At 50%load, 1200 rpm, the maximum ITE of 58.4 is achieved at injection timing of 8° aMinV that gives engine-out NOx of 40.0 g/kgf. At rated power conditions, ITE of 53.6 % is achieved at injection timing of -0.5° aMinV. Figure 24 shows in-cylinder pressure and heat released predictions for 9.8L engine for two load points, 50% load and 1200 rpm at injection timing of -8° aMinV and rated power at injection timing of -0.5° aMinV, respectively. At rated conditions, start of injection is delayed in order to keep PCP under 235 bar limit. Table 11 shows combustion performance parameters as predicted from CFD simulations for the two load points.

Optimized Factors from DoE model	
Compression Ratio [-]	Towards Higher Limit
Swirl Ratio [-]	Mid Range
Bowl parameter 1 [mm]	Towards Lower Limit
Spray inclusion angle [deg.]	Towards Higher Limit
Bowl parameter 2 [mm]	Towards Higher Limit
Bowl parameter 3 [mm]	Towards Mid-Range
Hole size [mm]	Towards Higher Limit
Rail Pressure[bars]	Towards Mid-Range
Start of Injection [deg. aMinV]	Towards Delayed Limit

Table 10: Optimized factors from DOE model predictor at a constant engine-out NO_x.

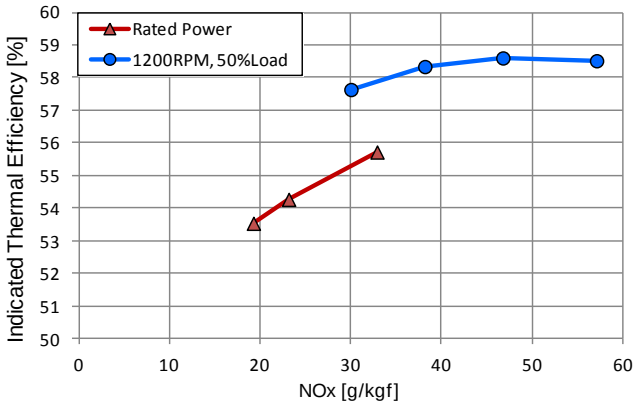

Figure 22: Start of injection sweeps at 50%load, 1200 rpm and 100%load, 1800rpm(Rated power condition) for optimized combustion system

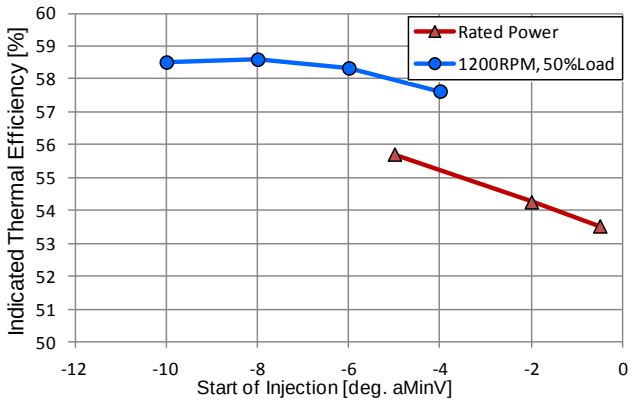

Figure 23: ITE vs SoI injection for 9.8L engine at 50%load, 1200 rpm and 100%load, 1800rpm(Rated power condition).

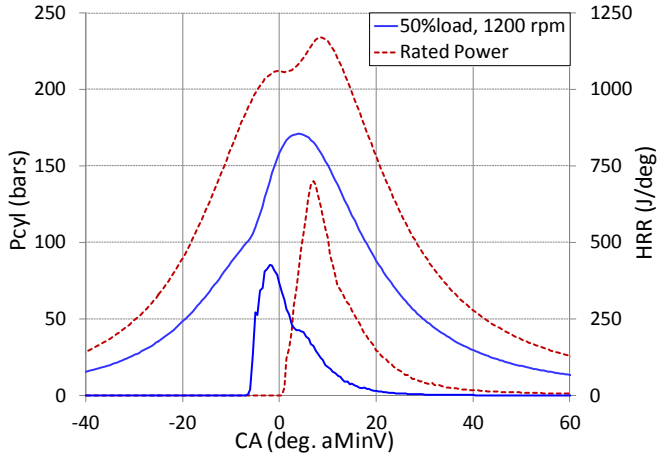

Figure 24: CFD predictions of in-cylinder pressure and instantaneous heat released rate at 1200 rpm, 50% load

9.8L_3-hole_0.37mm	Soot (gms/kgf)	NOx (gms/kgf)	Pdv_CC (kW)	CA10 (° ca)	CA50 (° ca)	CA90 (° ca)	CA1090 (° ca)	ITE [-]	PCP [bar]
50%load, 1200 rpm	0.003	50.4	50.8	-4.5	0.0	10.0	14.5	58.3	171
Rated Power	0.086	19.2	131.6	4.0	9.5	24.5	20.5	53.5	234

Table 11: CFD predictions of emission, burn duration and ITE at 1200 rpm, 50% load and rated power conditions for the 9.8L engine

Friction modeling and predictions

A detailed friction model analysis was performed for the OP 9.8L three-cylinder engine by using an analytical friction model that was validated for the 4.9L three-cylinder research engine as discussed previously in the paper. The major components of the engine such as the pistons, bearings, crank train and gearbox were sized for a 230 PCP limit in order to set the geometry required for the various sub-models of the friction model. The cylinder pressure trace obtained from GT-POWER was also used as an input for the friction model. A lube and water system model was created in LMS Amesim to determine flowrates and pressure requirements for these two operating conditions. Based on the assumption of a variable displacement pump, the flow and pressure requirement were converted in auxiliary power loss. The fuel pump power was calculated based on supplier data for the corresponding rail pressure, pump speed and fuel injection quantity. The total friction power loss and breakdown can be seen in Table 12. From the table it can be seen that the predicted friction power loss for the production 9.8L in 2020 time frame is expected to be much lower compared to current measured friction on 4.9L OP research engine. A portion of this improvement is obtained by optimizing the engine design for friction such as having an integrated gearbox with power take-off from exhaust crank and optimized size and design of engine components. Remaining reduction in friction is obtained by applying four-stroke technologies that have been published in literature and utilized in SuperTruck project. These include technologies listed below -

- Sputter coated bearings that are rated to unit loads of at least 120 MPa [36]
- Advanced piston ring coating that significantly reduce ring pack friction [37]
- Low friction polytetrafluoridethylene (PTFE) dynamic seals [38]

	Operating Conditions	
Engine [rpm]	1200	1800
Torque [N-m]	1017	1805
Power [kW]	128	340
Friction Power loss in components [kW]		
Main bearings [kW]	0.9	2.0
Water pump [kW]	0.1	1.1
Lube Oil Pump [kW]	0.7	1.4
Fuel Pump [kW]	1.2	5.7
Seals [kW]	0.1	0.1
FEAD [kW]	0.6	1.1
Total Aux & Crank [kW]	3.6	11.4
Rod bearings [kW]	0.6	1.3
Piston Skirt [kW]	1.2	4.5
Piston rings [kW]	2.3	6.1
PC+rod [kW]	4.2	11.9
Windage [kW]	0.3	1.3
GB bearings [kW]	0.1	0.1
Gear mesh	0.6	1.6
GB+windage [kW]	0.9	3.1
Total Friction Power [kW]	8.7	26.4

Table 12: Friction breakdown for 9.8L engine for part load and rated power point

BTE predictions

The results from the combustion CFD (heat release rate and ITE) along with the friction power loss were entered into the GT-POWER model. For the 1200 RPM 50% load condition, only the low pressure EGR was utilized and the high pressure EGR valve was closed. As a result, the turbocharger efficiency was sufficient to deliver boost, airflow and EGR outlined in Table 8 without requiring any additional supercharge work. For the rated power point, only high pressure EGR was utilized which results in about 2.5% pumping losses. Engine out NOx calculation is based on predicted NOx from combustion CFD. With SCR conversion efficiency of 95.8% at 1200 RPM 50% load and 91.5% at rated power, the tailpipe emissions can be met. As mentioned earlier, there is further possibility to improve performance at rated power by lowering EGR and boost and advancing start of injection. The combination of the thermal barrier coating, along with a liner designed to provide a trapped compression ratio of 21, and the proprietary combustion bowl of an OP Engine can provide a maximum brake thermal efficiency of 55.0% for the 9.8L HD engine – at 1200 RPM and 50% load condition. At the same time, the engine is able to deliver 340 kW with a brake thermal efficiency of 48% and with room for further optimization. Table 13 shows the prediction of pumping, friction loss and BTE for the two load points investigated. The 55% BTE corresponds to a 20% improvement compared to a heavy-duty 2014 DD15 multi-cylinder engine as published by National Highway Traffic Safety Administration (NHTSA) [39].

		1200RPM 6.5bar	1800RPM 11.6bar
Compressor Efficiency	%	79.5	81.6
Compressor Map PR	---	1.84	2.75
Turbine Efficiency (Aero + Mech)	%	73.7	69.1
Turbine Map PR	---	1.63	2.45
Turbine Rack Position	0 - 1	0.7	0.96
Total TC Efficiency	%	58.6	56.4
Supercharger Power	kW	0	17.7
BSFC	g/kW-hr	153.6	176.4
Engine Out BSNOx	g/kW-hr	6.5	3.2
Desired SCR conversion efficiency	%	95.8	91.5
IMEP	bar	6.9	13.4
Average PCP	bar	164	230
Brake Power	kW	128	342
Brake Torque	Nm	1016	1813
ITE	%	58.6	53.8
BTE	%	54.9	47.9
Friction/Fuel Power	%	3.7	3.4
Pumping/Fuel Power	%	0	2.5

Table 13: Predictions of Pumping, Friction and BSFC for 9.8L engine at 50% load, 1200 rpm and rated power conditions

The high efficiency results are achieved within the engine-out NO_x limit of 6.5 g/kW-hr at 1200rpm 6.5bar BMEP load, which is compatible with EPA 2010 emissions targets. These are the same targets for which the Department of Energy SuperTruck program was developed.

Given the uncertainty in future emissions regulations, it should be noted that this technology alternatively can be optimized to a much lower NO_x level to be compatible with future the proposed tail-pipe emission of 0.027 g/kW-hr NO_x.

Summary/Conclusions

Opposed-Piston engine models, viz., 3-D CFD, 1-D and friction models were correlated with measured data from dynamometer testing of the Achates Power 4.9L three-cylinder research OP Engine. The correlated models match the measurements and were extended to predict the heavy-duty 9.8 L three-cylinder OP Engine performance. For the air handling system design, port optimization was performed and a smaller port gave better scavenging performance. The combustion system was optimized using the design of experiment approach. CFD predictions at 1200rpm and 50% load show that an ITE of 58.4% can be achieved with use of a thermal barrier coating on both surfaces of the piston bowl. A 55% brake thermal efficiency is achieved at these conditions. At rated conditions with engine speed of 1800 rpm, BTE of 47.9% is achieved.

The OP Engine offers a solution in reducing GHGs emission and reducing the carbon foot-print for 2020 and beyond. It is demonstrated that OP Engine will reduce fuel consumption by providing BTE of 55% without the use of costly addition of technologies such as waste heat recovery systems or additional turbo-compounding components.

References

1. "EPA and NHTSA Propose Greenhouse Gas and Fuel Efficiency Standards for Medium- and Heavy-Duty Trucks: By the Numbers", https://www3.epa.gov/otaq/climate/documents/420f15903.pdf, EPA-420-F-15-903, June 2015.
2. Delgado, O, and Lutsey, N., " The U.S. SuperTruck Program: Expediting the development of Advanced heady-Duty Vehicle Efficiency Technologies", International Council of Clean Transportation, June 2014.
3. Koeberlein, D., "Technology and System Level Demonstration of Highly Efficient and Clean, Diesel Powered Class 8 Trucks," *http://energy.gov/eere/vehicles/vehicle-technologies-office-annual-merit-review-presentations*, DoE report, project ID: ACE057, 2015.
4. Singh, S., "Recovery Act – Class 8 Truck Freight Efficiency Improvement Project", *http://energy.gov/eere/vehicles/vehicle-technologies-office-annual-merit-review-presentations*, DoE report, project ID: ACE058, June 2015.
5. Zukouski, R., "SuperTruck – Development and Demonstration of a Fuel-Efficient Class 8 Tractor & Trailer Engine Systems", *http://energy.gov/eere/vehicles/vehicle-technologies-office-annual-merit-review-presentations*, DoE report, project ID: ACE059, 2016.
6. Amar, P., Gibble, J., " SuperTruck Powertrain Technologies for Efficiency Improvement", *http://energy.gov/eere/vehicles/vehicle-technologies-office-annual-merit-review-presentations*, DoE report, project ID: ACE060, 2016.
7. Hanson, R., Reitz, R.D., Splitter, D., and Kokjohn, S., "An Experimental Investigation of Fuel Reactivity Controlled PCCI Combustion in a Heavy-Duty Engine," SAE paper 2010-01-0864, SAE Int. J. Engines, Vol. 3, No.1, pp. 700-716, 2010.
8. Kokjohn, S.L., Hanson, R.M., Splitter, D.A., and Reitz, R.D., "Fuel Reactivity Controlled Compression Ignition (RCCI): A Pathway to Controlled High-Efficiency Clean Combustion," International Journal of Engine Research, Special Issue on Fuel Efficiency, Vol. 12, pp. 209-226, 2011.
9. Hanson, R., Ickes, A., and Wallner, T., "Comparison of RCCI Operation with and without EGR over the Full Operating Map of a Heavy-Duty Diesel Engine," SAE Technical Paper 2016-01-0794, 2016, doi:10.4271/2016-01-0794.
10. Manente, V., Zander, C., Johansson, B., Tunestal, P. et al., "An Advanced Internal Combustion Engine Concept for Low Emissions and High Efficiency from Idle to Max Load Using Gasoline Partially Premixed Combustion," SAE Technical Paper 2010-01-2198, 2010.
11. Chang, J., Kalghatgi, G., Amer, A., Adomeit, P. et al., "Vehicle Demonstration of Naphtha Fuel Achieving Both High Efficiency and Drivability with EURO6 Engine-Out NOx Emission," *SAE Int. J. Engines*6(1):101-119, 2013.
12. Sharma, A. and Redon, F., "Multi-Cylinder Opposed-Piston Engine Results on Transient Test Cycle," SAE Technical Paper 2016-01-1019, 2016
13. Regner, G., Herold, R., Wahl, M., Dion, E. et al., "The Achates Power Opposed-Piston Two-Stroke Engine: Performance and Emissions Results in a Medium-Duty Application," *SAE Int. J. Engines* 4(3):2726-2735, 201
14. Naik, S., Redon, F., Regner, G., and Koszewnik, J., "Opposed-Piston 2-Stroke Multi-Cylinder Engine Dynamometer Demonstration," SAE Technical Paper 2015-26-0038, 2015
15. Redon, F., Kalebjian, C., Kessler, J., Rakovec, N. et al., "Meeting Stringent 2025 Emissions and Fuel Efficiency Regulations with an Opposed-Piston, Light-Duty Diesel Engine," SAE Technical Paper 2014-01-1187, 2014
16. Venugopal, R., Abani, N., and MacKenzie, R., "Effects of Injection Pattern Design on Piston Thermal Management in an Opposed-Piston Two-Stroke Engine," SAE Technical Paper 2013-01-2423, 2013.
17. Herold, R., Wahl, M., Regner, G., Lemke, J. et al., "Thermodynamic Benefits of Opposed-Piston Two-Stroke Engines," SAE Technical Paper 2011-01-2216, 2011
18. Dion, E. P., Lenski, B. M.., and Mackenzie, R. G., "Piston constructions for opposed-piston engines" US 20120073526, 2012.
19. Senecal, P.K., Richards, K.J., Pomraning, E., Yang, T., Dai, M.Z., McDavid, R.M., Patterson, M.A., Hou, S., and Shethaji, T., "A New Parallel Cut-Cell Cartesian CFD Code for Rapid Grid Generation Applied to In-Cylinder Diesel Engine Simulations," SAE Paper No. 2007-01-0159, 2007.
20. Patel, A., Kong, S. C., and Reitz, R.D., "Development and Validation of a Reduced Reaction Mechanism for HCCI Engine Simulations," SAE Technical Paper 2004-01-0558, 2004.

21. Kong S.C., Sun Y., and Reitz R.D., Modeling diesel spray flame lift-off, sooting tendency and NOx emissions using detailed chemistry with phenomenological soot models, ASME J. Eng. Gas Turbines Power 129 (2007), pp. 245–251.
22. Smith G.P., Golden D.M., Frenklach M., Moriarty N.W., Eiteneer B., Goldenberg M., Bowman C.T., Hanson R.K., Song S., Gardiner W.C., Lissianski V.V., and Qin Z., 2000 [http://www.me.berkeley.edu/gri-mech/]
23. Hiroyasu, H., and Kadota, T., "Models for Combustion and Formation of Nitric Oxide and Soot in DI Diesel Engines," SAE Paper No. 760129, 1976.
24. Nagle, J., and Strickland-Constable, R.F., "Oxidation of Carbon Between 1000-2000 C," Proceedings of the Fifth Carbon Conference, Vol. 1, p.154, 1962.
25. Patterson, M.A., "Modeling the Effects of Fuel Injection Characteristics on Diesel Combustion and Emissions," Ph.D. Thesis, University of Wisconsin-Madison, 1997.
26. Abani, N., and Reitz, R.D., "Diesel engine emissions and combustion predictions using advanced mixing models applicable to fuel sprays", Combustion Theory and Modelling, Vol. 14, Iss. 5, pp 715-746, 2010.
27. O'Rourke, P.J., "Collective Drop Effects on Vaporizing Liquid Sprays," Ph.D. Thesis, Princeton University, 1981.
28. Han, Z., and Reitz, R.D., "Turbulence Modeling of Internal Combustion Engines Using RNG k-ε Models," Combustion Science and Technology, Vol. 106, 1995.
29. Klyza, C., "Optical Measurement Methods used in Calibration and Validation of Modeled Injection Spray Characteristics," Poster P7, presented in the 2010 Directions in Engine-Efficiency and Emissions Research (DEER) Conference.
30. Abani, N., Kokjohn, S., Park, S., Bergin, M. et al., "An Improved Spray Model for Reducing Numerical Parameter Dependencies in Diesel Engine CFD Simulations," SAE Technical Paper 2008-01-0970, 2008, doi:10.4271/2008-01-0970..
31. Taraza, D., Henein, N. A., Ceausu, R., and Bryzik, W., "Engine Friction Model for Transient Operation of Turbocharged, Common Rail Diesel Engines", SAE Technical paper 2007-01-1460, 2007.
32. Stanley, R., Taraza, D., Henein, N., and Bryzik, W., "A Simplified Friction Model of the Piston Ring Assembly", SAE Technical paper 1999-01-0974, 1999.
33. Taraza, D., Henein, N., and Bryzik, W., "Friction Losses in Multi-Cylinder Diesel Engines", SAE Technical Paper 2000-01-0921, 2000.
34. Hersey, M. D., "Theory and Research in Lubrication: Foundations for Future Developments", pp. 44-47, John Wiley & Sons, 1966.
35. "Gears – Thermal capacity, Part 2: Thermal load-carrying capacity," ISO/TR 14179-2:2001(E), First edition 2001-08-01, ISO 2001, 2001.
36. Praca, M., Uehara, S., Ferreira, M., and Mian, O., "New Polymeric Coating on Sputtered Bearings for Heavy-duty Diesel Engines," *SAE Int. J. Engines* 6(1):623-628, 2013, doi:10.4271/2013-01-1724.
37. Hoppe, S. and Kantola, T., "DuroGlide® - New Generation Piston Ring Coating for Fuel-Efficient Commercial Vehicle Engines," SAE Technical Paper 2014-01-2323, 2014, doi:10.4271/2014-01-2323.
38. Reichert, J., and Schäfer, P., "Reduced Friction in Engine Sealing System for Truck Engines," MTZ Worldw (2010) 71: 30. doi:10.1007/BF03227989
39. SwRI NHSTA 812194 report, *http://www.nhtsa.gov/Laws-&-Regulations/CAFE---Fuel-Economy/supporting-phase-2-proposal*, 2014.

Contact Information

Dr. Neerav Abani. Email: Abani@achatespower.com.
Address: 4060 Sorrento valley Blvd., San Diego CA92121. Tel: 858-535-9920.

Acknowledgments

Authors would like to thank Dr. Dave Foster, University of Wisconsin-Madison, and Dr. Gerhard Regner and John Koszewnik, Achates Power for continued discussions during the investigative study of the Achates Power 9.8L heavy-duty OP Engine.

Appendix

Definition of various scavenging parameters are shown in following equations

$$\text{Delivery Ratio (DR)} = \frac{\text{Mass of delivered air}}{\text{Displaced volume} \times \text{Ambient density}}$$

$$\text{Trapping Efficiency (TE)} = \frac{\text{Mass of delivered air retained}}{\text{Mass of delivered air}}$$

$$\text{Scavenging Efficiency (SE)} = \frac{\text{Mass of delivered air retained}}{\text{Mass of trapped cylinder charge}}$$

$$\text{Relative Charge (RC)} = \frac{\text{Mass of trapped cylinder charge}}{\text{Displaced volume} \times \text{Ambient density}}$$

$$\text{Charging efficiency (CE)} = \frac{\text{Mass of delivered air retained}}{\text{Displaced volume} \times \text{Ambient density}}$$

$$\text{Scavenging Ratio (SR)} = \frac{\text{Mass of delivered air}}{\text{Mass of trapped cylinder charge}}$$